Single-Particle Tracking: The Distribution of Diffusion Coefficients

Michael J. Saxton
Institute of Theoretical Dynamics, University of California, Davis, California 95616 and Laboratory of Chemical Biodynamics, Lawrence Berkeley National Laboratory, University of California, Berkeley, California 94720 USA

ABSTRACT In single-particle tracking experiments, the diffusion coefficient D may be measured from the trajectory of an individual particle in the cell membrane. The statistical distribution of single-trajectory diffusion coefficients is examined by Monte Carlo calculations. The width of this distribution may be useful as a measure of the heterogeneity of the membrane and as a test of models of hindered diffusion in the membrane. For some models, the distribution of the short-range diffusion coefficient is much narrower than the observed distribution for proteins diffusing in cell membranes. To aid in the analysis of single-particle tracking measurements, the distribution of D is examined for various definitions of D and for various trajectory lengths.

INTRODUCTION

The scatter in the observed diffusion coefficients of membrane proteins and lipids is of interest for two reasons, one technical and one biological. The technical reason is that in single-particle tracking (SPT) experiments, individual trajectories of mobile particles on the cell surface are observed, and a diffusion coefficient D can be obtained from a single trajectory. It is useful to know how good a value of a short- or medium-range diffusion coefficient can be obtained from a single trajectory with a given number of position measurements.

The biological reason to look at the scatter of D is to see the extent to which the scatter may reflect real heterogeneity in the membrane. A wide distribution of D is a common feature of fluorescence photobleaching recovery (FPR) measurements of lateral diffusion in cell membranes. Jacobson et al. (1984) found a 2-fold variation in D(FPR) from point to point on a single cell and a 10-fold variation among cells, and the variation among cells was not just due to the stage in the cell cycle. Wade et al. (1989) found the distribution of D to be lognormal and used the geometric mean as the value of D. The observed scatter in D is much greater than would be expected from the experimental error in an FPR experiment, implying heterogeneity of the membrane (Edidin, 1992; Feder et al., 1996; Ghosh and Webb, 1994; Jacobson et al., 1984; Thomas and Webb, 1990; Tocanne et al., 1994b). For reviews of other evidence of heterogeneity, see Bergelson et al. (1995), Edidin (1992, 1993, 1994), Jacobson and Vaz (1992), Tocanne et al. (1994a), and Welti and Glaser (1994).

The sources of the scatter in D may be biological, instrumental, or statistical. The goal is to see how much of the observed variation is purely biological. For a discussion of instrumental sources, see, for example, Petersen et al. (1986), Thomas and Webb, (1990), Gordon et al. (1995), and Munnelly et al. (1996). Here we examine the statistical component by Monte Carlo calculations. We consider a pure random walk, for which D is independent of time, and several models of diffusion with obstruction, binding, or both, for which D may be initially time dependent but crosses over to a time-independent value at large times (Saxton, 1995, 1996). We assume that diffusion does not follow a fractal time model (Nagle, 1992; Feder et al., 1996), for which $D(t) \sim t^{\alpha}$, $\alpha < 0$ for all times. We will not model here the scatter in the long-range diffusion coefficient from FPR experiments (see Schram et al., 1994, 1996).

In the first part of this article we consider the statistical scatter in D from Monte Carlo calculations and examine how it depends on the definition of D, the number of time points, and the statistical weighting. This work confirms and extends work of Qian et al. (1991) on the statistical accuracy of SPT. The results are of interest primarily to SPT experimentalists. The second part is of more general interest. It uses the scatter in D as a measure of the heterogeneity of a cell membrane, comparing the scatter measured in cells with the scatter obtained for various models of obstruction and binding.

Sources of heterogeneity may include lipid domains, binding sites on immobile species, trapping in coated pits (Kusumi et al., 1993), and obstruction by cytoskeletal elements. Hindered diffusion in cell membranes is discussed by Feder et al. (1996) and Kusumi and Sako (1996). For reviews of trapping models and hindered diffusion, see Bouchaud and Georges (1988, 1990), Haus and Kehr (1987), Havlin and Ben-Avraham (1987), and Scher et al. (1991).

METHODS

The Monte Carlo calculations are carried out as described earlier (Saxton, 1996). Briefly, mobile point obstacles are placed on a triangular lattice at random at a prescribed concentration. A tracer is placed at a random unblocked point on the lattice and carries out a random walk on unobstructed lattice sites. The tracer position is recorded as a function of time.

Received for publication 31 October 1996 and in final form 14 January 1997.

Address reprint requests to Dr. Michael J. Saxton, Institute of Theoretical Dynamics, University of California, Davis, CA 95616. Tel.: 916-752-6163; Fax: 916-752-7297; E-mail: mjsaxton@ucdavis.edu.

0006-3495/97/04/1744/10 $2.00

Periodic boundary conditions are imposed, and a 256 × 256 lattice is used. The modifications required to treat binding models are discussed elsewhere (Saxton, 1996). Thermal equilibrium initial conditions are assumed for the binding models. The approximations involved in a lattice model of lateral diffusion are discussed by Scalettar and Abney (1991) and Almeida and Vaz (1995).

In some of the calculations (indicated in the figure legends), a random-step-length continuum algorithm was used. At each time step, the direction of the step is chosen randomly, and the length of the step is chosen randomly from the distribution

$$(1/4\pi Dt)\exp(-r^2/4Dt)2\pi r dr$$

using the algorithm of Press et al. (1992). This distribution gives the radial displacement when a particle undergoes random independent Gaussian displacements in the x and y directions (Gnedenko, 1968). A slower alternative is to generate the random step as the sum of N steps of fixed length, scaled by $\sqrt{N}$; a value of $N = 32$ is safe. The continuum algorithm is preferable to a lattice model, because it eliminates from the histograms of D^* spikes that result from lattice structure.

Monte Carlo diffusion coefficients are denoted by D^*, normalized to 1 for pure unobstructed diffusion, and experimental diffusion coefficients are denoted by D. The "length of a trajectory" is used to indicate the number of position measurements for one particle, not a distance or a time.

RESULTS

We examine the probability distributions of short- and long-range diffusion coefficients obtained from individual trajectories. The results may seem artifactual, highly dependent on the definition of D^* and the length of the runs. But these are precisely the artifacts that arise in analysis of experimental SPT results, in which one has tens or hundreds of trajectories. The Monte Carlo calculations yield good probability distributions from well-defined models of hindered diffusion.

In SPT, the mean-square displacement (MSD) $\langle r^2(t)\rangle$ is calculated from an observed individual trajectory by internal averaging. Two methods (Qian et al., 1991) have been used, averaging over all pairs of points with a given time lag, and averaging over independent pairs of points with a given time lag. These averages are compared in detail in the Appendix. Here we use the averages over all pairs of points, because most experimentalists have done so. Averaging gives good values for short time lags and very scattered values for long time lags, so it is necessary to specify a cutoff time, that is, a maximum time lag used. For example, in a trajectory of 1024 time steps, if the averaging is done over independent pairs of points 512 time steps apart, there are only two pairs in the average, $[r(512) - r(0)]^2$ and $[r(1024) - r(512)]^2$, and the scatter in $\langle r^2(512)\rangle$ is large. If the averaging is done over all pairs of points 512 time steps apart, there are 512 pairs in the average, $[r(512) - r(0)]^2$, $[r(513) - r(1)]^2, \ldots, [r(1024) - r(512)]^2$, but the pairs are highly correlated, and the scatter in $\langle r^2(512)\rangle$ is still large.

Averaging is necessary, but it can obscure transitions between Brownian and non-Brownian motion. It is necessary to analyze $r^2(t)$ to establish the mode of motion, and if the motion is diffusive, it is then appropriate to look at the short-range diffusion coefficient.

Scatter

The necessity of averaging is illustrated in Fig. 1. We consider a random walk of 1024 time steps on a triangular lattice with random point obstacles. The geometry is fixed; in each run, a single obstacle configuration and a single starting point are used, and D^* is calculated as a function of the number of trajectories N_{TRAJ} averaged over. Five runs are shown for each obstacle concentration, $C = 0.0$ and $C = 0.3$, and for $C = 0.3$ the obstacle configuration is varied among the five runs.

In Fig. 1 *a*, no internal averaging is used, and D^* is obtained from an unweighted least-squares fit to $\langle r^2(t)\rangle$ averaged over N_{TRAJ} trajectories. For N_{TRAJ} small, the scatter is large, and the diffusion coefficients for $C = 0.0$ and $C = 0.3$ cannot be distinguished reliably. For $N_{TRAJ} \sim 10^2$, the scatter is much less, the difference in D^* for the two obstacle concentrations is unequivocal, and the numerical values are reasonable. For N_{TRAJ} large, D^* converges to its limiting value; the small scatter for $C = 0.3$ is due to the different obstacle configurations in the five runs.

The situation improves considerably when internal averaging is used, as shown in Fig. 1 *b*. Again the runs are 1024 time steps long, but here the least-squares fit is to $\langle r^2(t)\rangle$

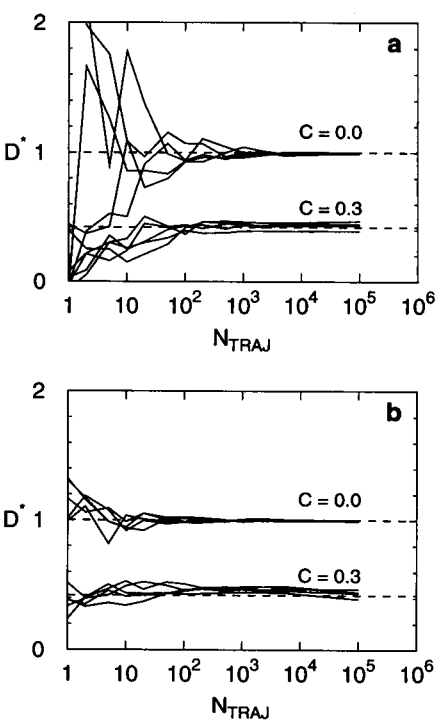

FIGURE 1 Dependence of the diffusion coefficient D^* on the number of trajectories N_{TRAJ} averaged over. Random walks were carried out for five independent runs of 1024 time steps on an unobstructed triangular lattice ($C = 0.0$) or in the presence of immobile random point obstacles ($C = 0.3$). For $C = 0.3$, the scatter in D^* for large N_{TRAJ} is due to variation in obstacle geometry among the five runs. (*a*) Averaging only over N_{TRAJ} trajectories. An unweighted least-squares fit to all 1024 points was used. (*b*) Averaging over all pairs of points and over N_{TRAJ} trajectories, with a cutoff time of 128. Dotted lines indicate limiting values of D^* for a large number of trajectories.

averaged over all pairs of points and over N_{TRAJ} trajectories, with a cutoff time of 128. There is no ambiguity; $C = 0.0$ and $C = 0.3$ can be distinguished easily, even for a single trajectory. The figure shows the average over all pairs of points; averaging over independent pairs of points gives very similar results. If the cutoff time is 256, the scatter increases, but the two obstacle concentrations can still be distinguished. If the cutoff time is 512, the scatter is similar to that in Fig. 1 *a*.

Definitions of diffusion coefficients

In SPT experiments, a typical trajectory consists of 20–2000 position measurements. The number of position measurements may be limited by internalization of the label, motion out of the focal plane, photobleaching, or a transition to nondiffusive motion. In examining trajectories of these lengths, the definition of the diffusion coefficient is important. Short- and long-range diffusion coefficients are in fact distinct, with different averages except in the case of unobstructed diffusion, and different probability distributions in all cases. Typically in SPT a short-range D is measured, over distances of tens of nanometers, to find a value as independent as possible of directed motion, obstacles, and corral boundaries. In contrast, FPR experiments measure a long-range D, over a range of a few micrometers.

How does the distribution of D^* depend on the definition of D^* if the number of time points is fixed? We generate a trajectory of $N_T = 1024$ time steps, find the MSD for all time lags 0–1024, and calculate $D^*(0{:}N_D)$ from an unweighted least-squares fit of a line to lags 0–N_D. In the fit, the origin is included as a data point, but the least-squares line is not constrained to pass through the origin. As Fig. 2 shows, if the fit includes all 1024 points, the distribution of D^* is extremely wide and includes negative values of D^*. As N_D is decreased, the distribution becomes much narrower. The short-range diffusion coefficients $D^*(0{:}\,4)$ and $D^*(0{:}\,8)$ are well determined; the longest-range diffusion coefficients $D^*(0{:}\,512)$ and $D^*(0{:}\,1024)$ are so broadly distributed as to be useless. Fig. 2 *a* shows the distributions for unobstructed diffusion; Fig. 2 *b*, for obstructed diffusion with an obstacle concentration $C = 0.3$. For $C = 0.0$, the average value $\langle D^* \rangle = 1$ for all definitions of D^*, but for $C = 0.3$, the average decreases as N_D increases.

Dependence on run time

Next, we hold the definition of D^* constant and vary the number of time points in the trajectory. A short-range diffusion coefficient $D^*(0{:}\,4)$ was used, and the length of the runs was varied from 4 to 1024 time steps. For short trajectories the distribution is so wide that measurements of D are useless. As the length of the runs increases, the distribution of D^* becomes much narrower. The standard deviations σ of the distributions in Figs. 2 and 3 agree closely with the values from the formula of Qian et al.

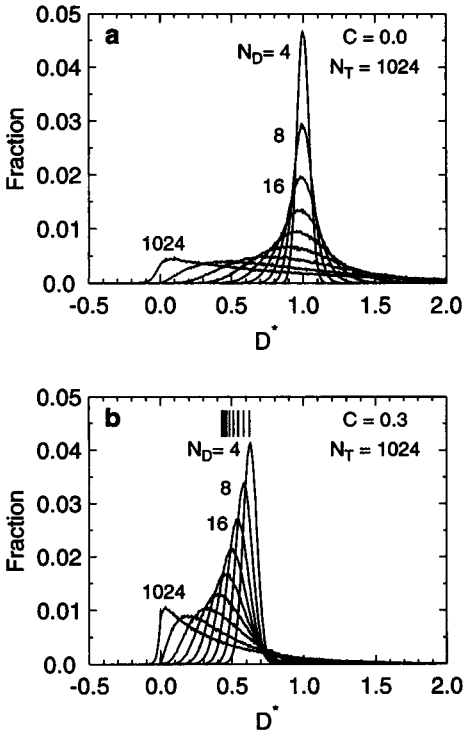

FIGURE 2 Distributions of the diffusion coefficient $D^*(0{:}\,N_D)$ for various definitions of the diffusion coefficient. Random walks were carried out for $N_T = 1024$ time steps on an unobstructed triangular lattice (*a*, $C = 0.0$) or in the presence of immobile random point obstacles (*b*, $C = 0.3$). Diffusion coefficients were obtained from an unweighted least-squares fit to the MSD for the first $N_D = 4, 8, 16, \ldots, 1024$ values of $\langle r^2(t) \rangle$. Vertical bars in (*b*) indicate the average D^*.

(1991): $\sigma/D = [2N_D/3(N_T - N_D)]^{1/2}$, unless $N_T \to N_D$. These results indicate the importance of making the longest series of measurements possible. In fluorescence SPT measurements, efforts to reduce photobleaching of label are essential.

The families of curves in Figs. 2 *a* and 3 are very similar. In fact, the Monte Carlo results show that for an unob-

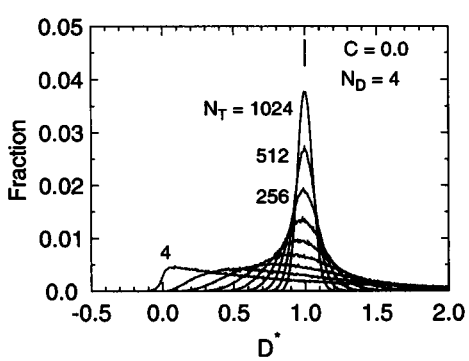

FIGURE 3 Distributions of the short-range diffusion coefficient $D^*(0{:}\,4)$ for trajectories with various numbers of time points. Random walks were carried out for $N_T = 4, 8, 16, \ldots, 1024$ time steps for a continuum random walk with random step size, and D^* was obtained from an unweighted least-squares fit to the MSD for the first $N_D = 4$ time points. Vertical bars indicate the average D^*.

structed random walk, if the number of points in the least-squares fit is N_D and the length of the run is N_T, then to a good approximation the distribution of $D^*(0: N_D)$ depends only on the ratio N_D/N_T.

Effect of weighting

So far, unweighted least-squares fits have been used to find D^*. But weighting is appropriate because the values of the MSD are known much more precisely for short time lags than for long ones. The weights w values in the least-squares fit are inversely proportional to the variance of $\langle r^2 \rangle$ for each t (Bevington and Robinson, 1992). Formulas for the variance (Qian et al., 1991) are summarized in the Appendix, and a plot of the weights for a trajectory of 1024 time steps is shown. The least-squares fit includes the point $\langle r^2(0) \rangle = 0$, which is known exactly. We somewhat arbitrarily choose $w(0) = w(1)$. Small lags are weighted heavily, so the weighted D^* is a short-range diffusion coefficient, whatever definition of D^* is chosen. The distributions for various definitions of D^* are shown in Fig. 4 for the same conditions as in Fig. 2. The distributions for the weighted D^* are much narrower than those for the unweighted D^*.

Dependence on concentration

Next, we consider the concentration dependence of the distribution of D^* for diffusion in the presence of random point obstacles. As expected, for typical trajectory lengths SPT gives good short-range diffusion coefficients but poor long-range ones. Fig. 5 *a* shows the distribution of short-range diffusion coefficients, $D^*(0: 4)$, for diffusion on the triangular lattice in the presence of random point obstacles at various concentrations. The distributions are Gaussian to a good approximation, in agreement with results for long-range diffusion coefficients for the cubic lattice (Braun and Kehr, 1990). For $C \sim 0.5$ there is a small non-Gaussian tail in the distribution, resulting from tracers that are trapped on finite clusters and therefore have a low D^*. Fig. 5 *b* shows the distributions for a medium-range diffusion coefficient $D^*(0: 128)$. There is much more overlap than for $D^*(0: 4)$, and one could not distinguish the slowest trajectories for $C = 0$ from the fastest trajectories for $C = 0.5$.

We examine short- and medium-range diffusion coefficients obtained from trajectories of 1024 time steps, so we cannot discuss the fluctuations in the long-range diffusion coefficient near the percolation threshold. For $D^*(0: 4)$, the width of the distribution increases moderately as the obsta-

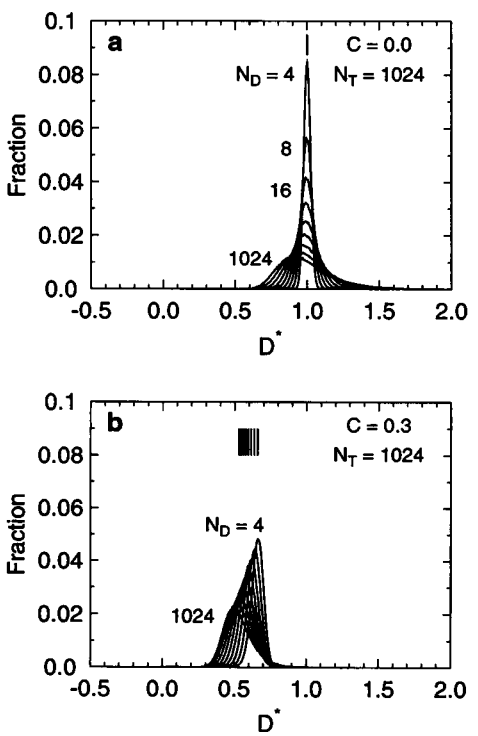

FIGURE 4 Distributions of the diffusion coefficient D^* for various definitions of D^* for weighted averages. Random walks were carried out for $N_T = 1024$ time steps on an unobstructed triangular lattice (*a*, $C = 0.0$) or in the presence of immobile random point obstacles (*b*, $C = 0.3$). Diffusion coefficients were obtained from a weighted least-squares fit to the MSD for the first $N_D = 4, 8, 16, \ldots, 1024$ values of $\langle r^2(t) \rangle$. This figure is directly comparable to Fig. 2 but with a change in vertical scale. Vertical bars indicate the average D^*.

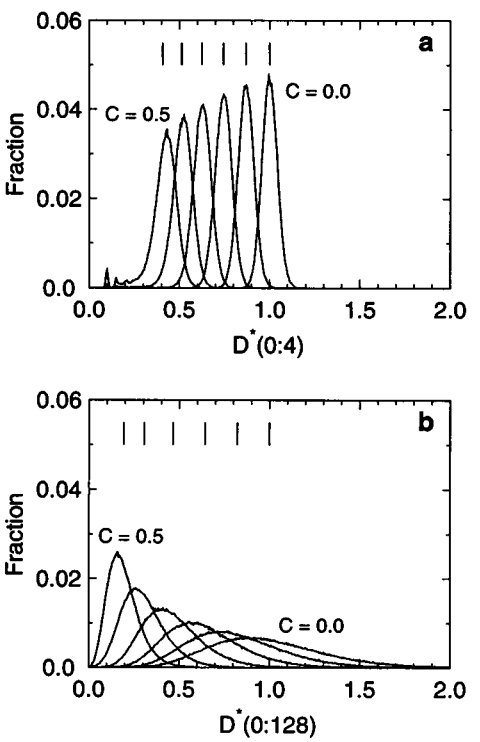

FIGURE 5 Distribution of diffusion coefficients for a random walk of 1024 time steps on the triangular lattice with random point obstacles at concentrations $C = 0.0, 0.1, 0.2, 0.3, 0.4$, and 0.5. Averaging over all pairs is used but without statistical weighting. Vertical lines indicate the average D^*. (*a*) Distribution of short-range diffusion coefficients $D^*(0: 4)$. (*b*) Distribution of the medium-range diffusion coefficient $D^*(0: 128)$. Here the tracers are restricted to the percolating cluster for $C \geq 0.3$, so there are no tails at small D^*.

cle concentration increases; the width at the percolation threshold $C = 0.5$ is 30% greater than at $C = 0$.

For obstructed diffusion, there are two sources of scatter in D^*, the randomness of the random walk and the variations in obstacle configuration among measurements. Fig. 1 *a* showed a small variation in D^* for five different obstacle configurations with $C = 0.3$ in the limit of a large number of trajectories. We can examine this more systematically by calculating $D^*(0: 4)$ and $D^*(0: 128)$ for a fixed obstacle configuration and a fixed initial point, but averaged over a large number of trajectories. We then compile histograms of the two diffusion coefficients for different random configurations of obstacles. In Fig. 6, the narrow histograms include only the scatter due to the variation in obstacle configuration, and the wide histograms include both sources of scatter. For the short-range diffusion coefficient, $D^*(0: 4)$, the two sources of scatter are of similar magnitude, but for the medium-range diffusion coefficient, $D^*(0: 128)$, the contribution from variation in obstacle configuration is relatively small.

Biological variability and trapping models

In the second part of this article we consider the biological question of the inhomogeneity of the membrane. We compare the observed distribution of short-range D in cells with the Monte Carlo distribution for various models of obstruction and binding, and find that some models of hindered diffusion can be excluded.

We use the observed distribution for E-cadherin in cultured mouse keratinocytes in high-calcium medium (Kusumi et al., 1993, Fig. 5). Kusumi et al. classified the modes of motion for E-cadherin in this medium as 28% simple diffusion, 64% restricted motion, 2% directed motion, and 6% stationary. The distribution is typical of their results. For high-calcium medium, the distributions of modes of motion for E-cadherin, the epidermal growth factor receptor, and the transferrin receptor were very similar. For the three proteins, the distributions of D for restricted diffusion were all two orders of magnitude wide and for simple diffusion the distributions were at least one order of magnitude wide (Kusumi et al., 1993, Fig. 11). In low-calcium medium, 59% of the E-cadherin is in the directed and stationary modes; the difference in modes of motion is attributed to attachment of E-cadherin to cytoskeletal elements, including motor proteins. The distribution of diffusion coefficients in the low-calcium case is slightly wider than in the high-calcium case.

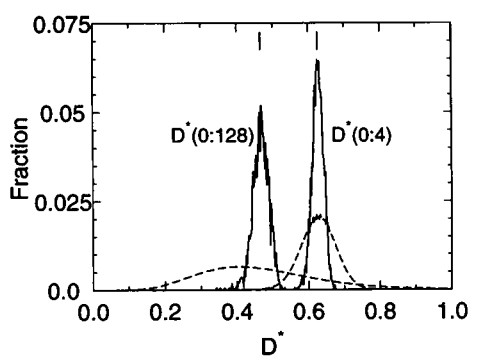

FIGURE 6 Distributions of the short-range diffusion coefficient $D^*(0: 4)$ and the medium-range diffusion coefficient $D^*(0: 128)$ for a random walk of 1024 time steps on the triangular lattice with random point obstacles at a concentration $C = 0.3$. Solid lines indicate the distribution due to variation in obstacle configuration alone. Values of D^* were obtained by averaging 2000 trajectories at a fixed obstacle configuration and initial position, and the histogram includes 2500 different obstacle configurations. A run with 5000 trajectories per obstacle configuration gave similar results. Dotted lines indicate the distribution due to both variation in obstacle configuration and variation among random walks, calculated from single trajectories. In both cases, trajectories were averaged over all pairs, and no weighting was used.

We consider several models of hindered diffusion, summarized here and discussed in detail elsewhere (Saxton, 1995, 1996). The initial condition is assumed to be thermal equilibrium, as is presumably appropriate in most membrane experiments (Saxton, 1996).

Three of the models involve random point obstacles. The first is random point obstacles with no binding, the reference case already considered. The second is the uniform obstruction/binding model, in which a tracer is bound by an obstacle in a nearest neighbor site, but the binding energy is unchanged if the tracer is adjacent to more than one obstacle. The third is the variable obstruction/binding model, in which tracers are bound by nearest neighbor obstacles, but each adjacent obstacle contributes an equal binding energy. This model includes deep wells; for the triangular lattice, the escape probabilities are between P_{ESC} and P_{ESC}^5, where P_{ESC} is the probability of escape in an unobstructed move from a single adjacent obstacle. The two obstruction/binding models are quantitative forms of the "post model" of Zhang et al. (1993). The fourth model has no obstacles, but each site is assigned an escape probability W from a power law distribution $P(W)\,dW = (1 - \alpha)\,W^{-\alpha}\,dW$ with $0 \leq \alpha < 1$. It is a singular distribution, with a nonzero probability of any waiting time, however large.

These models are all valley models, in which the tracer moves from site to site on a lattice and falls into wells of various depths at the sites. The tracer does not know the depth of a well before it enters. Another possibility is a mountain model, in which all the sites are at zero energy and the barriers are on the bonds joining the sites. Mountain and valley models are qualitatively much different. In a valley model, deep wells have a major effect when tracers are trapped in them, and in thermal equilibrium, tracers are likely to be trapped in deep wells initially. In contrast, in a mountain model, the thermal equilibrium distribution is uniform, and a tracer is likely to go around a high barrier (Bunde, 1988). So a high barrier in the mountain model has much less effect than a deep well in the valley model.

To compare experimental and calculated distributions, we use $D^*(2: 4)$, the short-range diffusion coefficient used by Kusumi et al. (1993). A short-range D^* has the advantages that it is accurately obtained and the influence of

directed and confined motion is minimized. The distribution of $D^*(2: 4)$ is wider than that of $D^*(0: 4)$, but Kusumi et al. (1993) found $D^*(2: 4)$ advantageous for analyzing experimental data. The range of D is wide enough that it is convenient to plot the distribution of log D (Kusumi et al., 1993). Trajectories for which $D = 0$ are not included in the histograms; these would be part of the immobile fraction in either SPT or FPR measurements. There are 1000 time steps in the experimental trajectories and 1024 in the Monte Carlo trajectories.

We show the Monte Carlo results in detail to demonstrate that the width of the distribution is primarily dependent on the binding model and only secondarily dependent on the parameters of the binding model. All the results are shown on the same horizontal scale so that they can be compared directly, but two vertical scales had to be used. The experimental distribution (Fig. 7 *a*) is greater than two orders of magnitude wide. Clearly random point obstacles (Fig. 7 *b*) cannot account for this distribution; the whole family of distributions is less than one order of magnitude wide. Similarly, the mountain models are inadequate; they are at most an order of magnitude wide (Fig. 7 *c*). The distributions shown in Fig. 7 *c* are for a uniform distribution of barrier energies with the transition rate given by an Arrhenius factor; distributions for a power law distribution of transition rates are similar. The simplest valley model, the uniform obstruction/binding model, gives distributions approximately one order of magnitude wide (Fig. 7 *d*), too narrow except at very low P_{ESC}. But the variable obstruction/binding model (Fig. 7 *e*) gives a width similar to that observed. The lowest escape probability possible is P_{ESC}^5; therefore, this model is not singular, but some wells are very deep. Similarly, the power law distribution of escape probabilities (Fig. 7 *f*) has an appropriate width. This valley model is in fact singular. (For the power law distribution, the long-range diffusion coefficient decreases as the system size increases (Saxton, 1996). The larger the system, the deeper the deepest well is likely to be. But in a run of 1024 time steps, all well depths with $P_{ESC} \ll 1/1024$ are practically equivalent. In a short run, as the system size increases, the distribution of diffusion coefficients for the mobile fraction is the same, but the immobile fraction increases.)

Clearly this sort of comparison cannot prove that a given model is correct, but it can disprove models. Here it suggests that the membrane must have at least as much inhomogeneity as the valley models with a wide distribution of well depths. Although the effects of directed motion and corral walls can be reduced by using a short-range diffusion coefficient, one cannot reduce the effects of binding. Binding sites are local features and affect the microscopic diffusion coefficient.

DISCUSSION

A common view among FPR experimentalists is that the observed scatter in long-range FPR diffusion coefficients is much larger than expected from experimental error, and this discrepancy implies heterogeneity in the membrane (Edidin, 1992; Feder et al., 1996; Ghosh and Webb, 1994; Jacobson et al., 1984; Thomas and Webb, 1990; Tocanne et al., 1994b). The scatter in short-range SPT diffusion coefficients is likewise large (Kusumi et al., 1993; Lee et al., 1991, 1993; Sako and Kusumi, 1994). It is therefore useful to examine the distribution of D for various models of hindered diffusion. Comparison of observed short-range D values with the models indicates that the simple obstruction model and the two mountain models do not give distributions as wide as those observed. The uniform obstruction/binding model would require a large binding energy. With appropriate choices of parameters, valley models with extreme well depths—the variable obstruction/binding model and the power law distribution of well depths—are able to give distributions similar to those observed. The width of the distribution alone is not sufficient to demonstrate which model is correct, but it provides a useful constraint. Models of hindered diffusion have at least one free parameter, such as an obstacle concentration, a well depth distribution exponent, or a binding energy, so it is hard to rule out any model on the basis of D alone. The distribution of D provides another prediction to compare with experiment.

Scatter in the observed D should be viewed as signal as well as noise. Experimentalists should publish histograms of D and the immobile fraction for both FPR and SPT experiments (Tocanne et al., 1994b). It would be useful to have SPT measurements of the distribution of diffusion coefficients for single-component artificial bilayers well above the gel-fluid transition to provide an estimate of the scatter in D due to instrumental stability and error in position measurements.

The Monte Carlo calculations presented here have several implications for analysis of SPT data. Foremost, the results show that with the usual number of data points in trajectories, one can get good short-range diffusion coefficients but not good long-range ones. Averaging is necessary, although it should not be done automatically, because it may confound diffusive and nondiffusive segments of a trajectory. As discussed in the Appendix, averaging over all pairs of points is preferable to averaging over independent pairs of points, although the difference is small, and neither average is able to reduce low-frequency fluctuations significantly at large time lags. There are simply not enough data points at large time lags to give a reliable value of the MSD, and the trajectory should be cut off at approximately one-quarter of the total number of data points. In least-squares fits to the MSD, the appropriate statistical weighting factors should be used (Qian et al., 1991), in their analytical form without approximation. The use of the weighting factors automatically enforces the cutoff for large time lags.

For an unobstructed random walk, a least-squares fit with no averaging yields an extremely wide distribution of diffusion coefficients, including negative ones (Fig. 2), yet the average is $\langle D^* \rangle = 1$. The variation among trajectories is large, and all of the trajectories are legitimate random

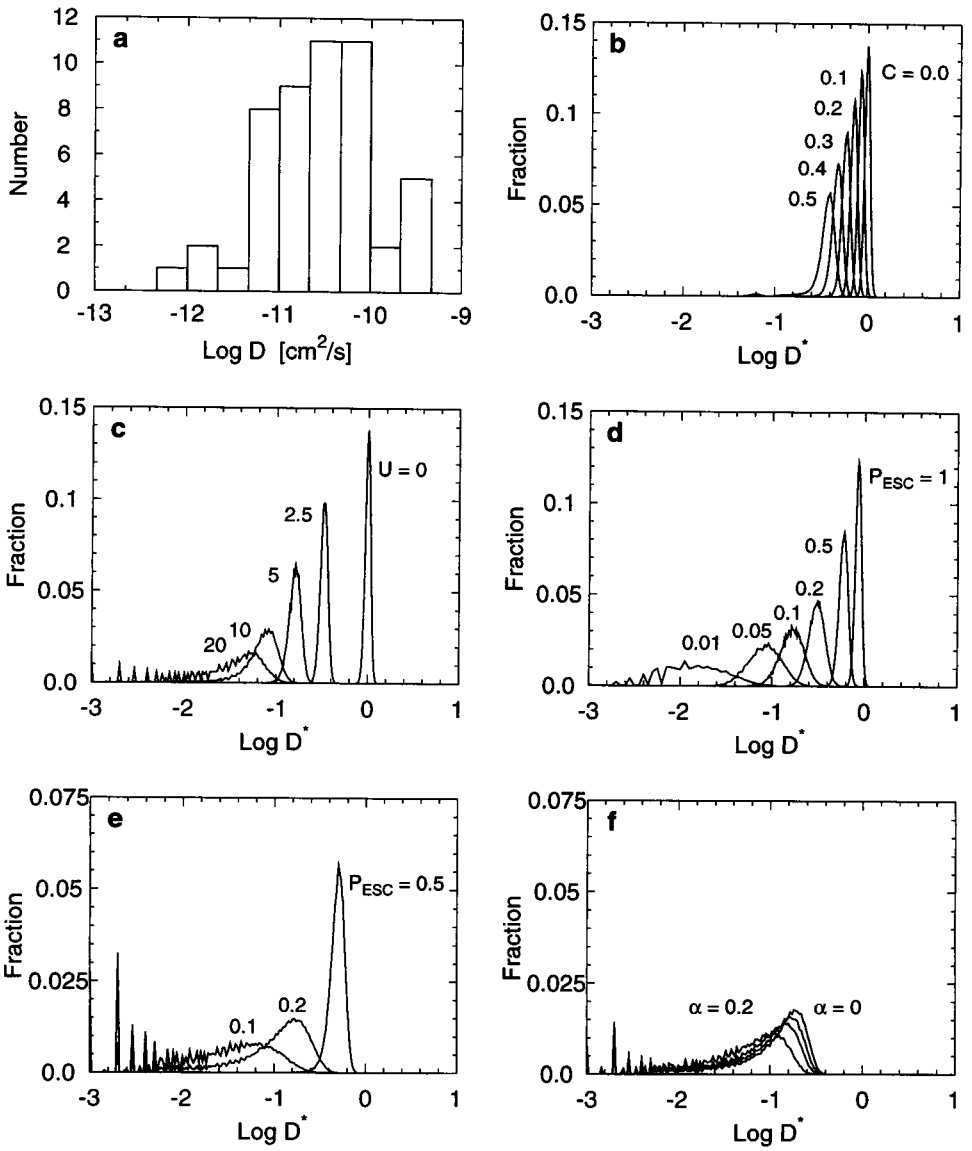

FIGURE 7 Distribution of log $D(2: 4)$ for various diffusion models and for SPT measurements of diffusion of E-cadherin in keratinocytes in high-calcium medium (Kusumi et al., 1993). All distributions are shown on the same horizontal scale. For the models, all runs are for 1024 time steps, and $D^*(2: 4)$ is found by an unweighted least-squares fit to the MSD averaged over all pairs. Thermal equilibrium initial conditions are used. At least 100 configurations of obstacles or traps and at least 2000 trajectories per configuration are used. (*a*) Experimental data for $D(2: 4)$ for E-cadherin in a cultured mouse keratinocyte in high-calcium medium. The motion is predominantly simple and restricted diffusion. The label is colloidal gold 40 nm in diameter coated with a monoclonal antibody (Kusumi et al., 1993). (*b*) Random point obstacles on a triangular lattice at concentrations $C = 0.0$, 0.1, 0.2, 0.3, 0.4, and 0.5. (*c*) Mountain model with a uniform distribution of barrier heights. Each bond on a triangular lattice is assigned a random energy uniformly distributed on $[0,U]$, and the transition probability for that bond is obtained from an Arrhenius factor $\exp(-U/kT)$. Values of U are 0, 2.5, 5, 10, and 20 in units of kT. The spikes in the histograms for large U result from the use of a lattice model of diffusion and would disappear in a continuum model with random step size and a continuous potential representing the barriers. For clarity, in several histograms the bin width has been varied to reduce the spikes; the histograms are normalized to the same area. (*d*) Uniform obstruction/binding model, a valley model, for obstacle concentration $C = 0.1$ and the indicated values of the escape probability, P_{ESC}, the value for escape from an isolated trap. Random point obstacles on a triangular lattice obstruct motion and bind tracers in nearest neighbor sites, but the binding energy at a site is independent of the number of adjacent obstacles. The limit $P_{ESC} = 1$ corresponds to obstructed diffusion with no binding (*b*, $C = 0.1$). (*e*) Variable obstruction/binding model, a valley model. Random point obstacles on a triangular lattice obstruct motion and bind tracers in nearest-neighbor sites, and each adjacent obstacle contributes an equal binding energy to the tracer. The obstacle concentration is $C = 0.1$, and $P_{ESC} = 0.1$, 0.2, and 0.5. As P_{ESC} decreases, the immobile fraction for 1024 time steps increases from 0.000 to 0.086 to 0.560. In the limit $P_{ESC} = 1$, this model gives the distribution for $C = 0.1$ in (*a*), too high to be shown. (*f*) Power law distribution of escape probabilities. This is a valley model with a singular distribution of escape probabilities. Here the exponent $\alpha = 0$, 0.05, 0.10, and 0.20. The curve for $\alpha = 0$ is not free diffusion but diffusion in which the escape probability from each lattice site is a random number uniformly distributed on (0,1). The escape probability may be arbitrarily low, so the immobile fraction is large. In these runs, 47–84% of the tracers were immobile for the 1024 time steps, and another 2–4% had diffusion coefficients below 10^{-3}. The number of deep wells is small, but with thermal equilibrium initial conditions, tracers are likely to be in these wells initially.

walks. One must be careful in rejecting trajectories as nondiffusive; by suitable editing of trajectories one can get D^* to be practically anything. If some trajectories are rejected as nondiffusive, one should apply the same rejection procedure to unobstructed continuum random walks and examine the resulting average D^* and distribution of D^*.

APPENDIX

Internal averaging

To determine a diffusion coefficient from a single trajectory, it is necessary to calculate the MSD. The calculation of the MSD should not be done automatically. If the observed particle changes its mode of motion during the trajectory, calculation of the MSD may yield misleading results. Transitions between Brownian motion and directed or hindered motion are often observed in SPT measurements on cells (for review, see Saxton and Jacobson, 1997).

There are two ways to calculate the MSD for a given time lag Δt, by averaging over all pairs of points Δt time steps apart, or by averaging over independent pairs of points Δt time steps apart (Qian et al., 1991). Most workers use the average over all pairs, but some (Ghosh, 1991; Slattery, 1995; Feder et al., 1996) use the average over independent pairs, on the grounds that each segment is then an independent, nonredundant random walk. The average over independent pairs of points has the advantage that the probability distribution of this average is simply a gamma distribution (Qian et al., 1991). It is useful to examine the difference between the two averages in detail.

Consider the MSD $\langle r^2(n)\rangle$ calculated for a trajectory $\vec{r}(t)$ of $N_T + 1$ time steps including the initial position $\langle r^2(0)\rangle$, where the time n is expressed in units of δt, the acquisition time for one video image. Then there are $N_I = \lfloor N_T/n \rfloor$ nonoverlapping segments of length n, where $\lfloor\ \rfloor$ is the greatest integer function. The average over independent pairs is

$$\langle r^2(n)\rangle_I = \frac{1}{N_I}\sum_{i=1}^{N_I}[\vec{r}(ni) - \vec{r}(ni - n)]^2. \qquad \text{(A1)}$$

There are $N_A = N_T - n + 1$ overlapping segments of length n, and the average over all pairs is

$$\langle r^2(n)\rangle_A = \frac{1}{N_A}\sum_{i=0}^{N_A-1}[\vec{r}(i + n) - \vec{r}(i)]^2. \qquad \text{(A2)}$$

For $n = 1$ and $n = N_T$, the averages are identical.

The pattern of data collection, shown in Fig. A1, strongly supports the use of the average over all pairs. In the average over all pairs, the sampling is uniform except for end effects. But in the average over independent pairs, trajectory points are sampled differently depending on how many prime factors the number of the time step has. For example, trajectory point 5 is used in calculating $\langle r^2(n)\rangle$ only for $n = 1$ and 5. Trajectory point 6 is used for $n = 1, 2, 3$, and 6, but trajectory point 7 is used only for $n = 1$ and 7. The bias is worse for, say, $n = 59, 60, 61$. Furthermore, the average over all pairs does not waste the stray ends of trajectories. In calculations of the MSD for a time lag of 257 in a trajectory of 1024 time points, the average over independent pairs uses three pairs of points and throws away all points beyond 3×257, but the average over all pairs uses those discarded points.

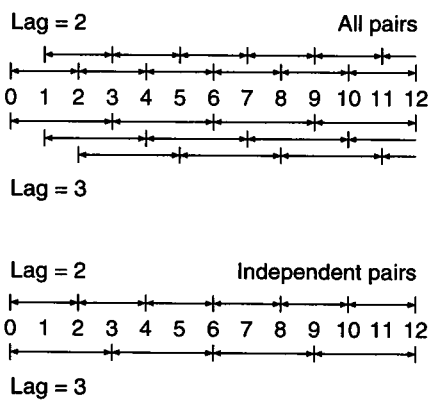

FIGURE A1 Patterns of sampling for averages over all pairs and averages over independent pairs of trajectory points for lags of 2 and 3 time steps.

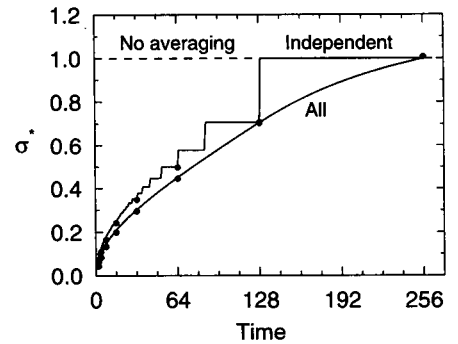

FIGURE A2 Normalized standard deviations σ^* for averages over all pairs and all independent pairs for a 256-step random walk. The horizontal line indicates the value for an unweighted random walk. Points indicate Monte Carlo results for a continuum random walk with a random step size.

But using the average over all pairs instead of the average over all independent pairs does not improve the signal-to-noise ratio much, because the overlapping pairs are highly correlated. For an unaveraged two-dimensional random walk, the probability density is (Carslaw and Jaeger, 1959)

$$C(r, t) = (1/4\pi Dt)\exp(-r^2/4Dt), \qquad \text{(A3)}$$

so the MSD is $\langle r^2(t)\rangle = 4Dt$, the variance is

$$\text{Var}\,\langle r^2\rangle = (4Dt)^2, \qquad \text{(A4)}$$

and the SD is equal to the MSD. For an average over N_I independent segments, $z = \langle r^2\rangle_I$ is given by a gamma distribution (Qian et al., 1991)

$$P(z)dz = \frac{1}{\Gamma(N_I)}u^{N_I-1}e^{-u}du, \qquad \text{(A5)}$$

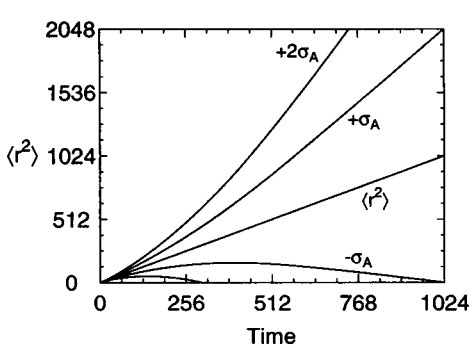

FIGURE A3 The mean value $\langle r^2(t)\rangle$ for a random walk, $\langle r^2(t)\rangle \pm \sigma_A$, and $\langle r^2(t)\rangle \pm 2\sigma_A$, where σ_A is the SD for averages over all pairs. These are in dimensionless units (Saxton, 1996) in which $\langle r^2\rangle = t$.

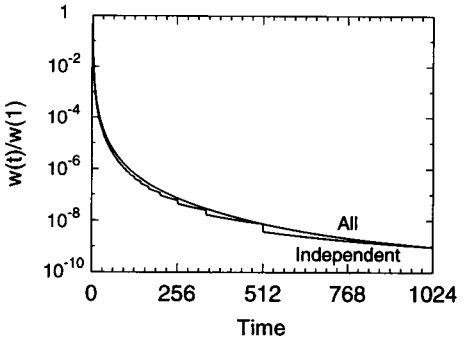

FIGURE A4 Statistical weights w for the MSD in a trajectory of 1024 time points, normalized to one for the first point, from the formulas of Qian et al. (1991).

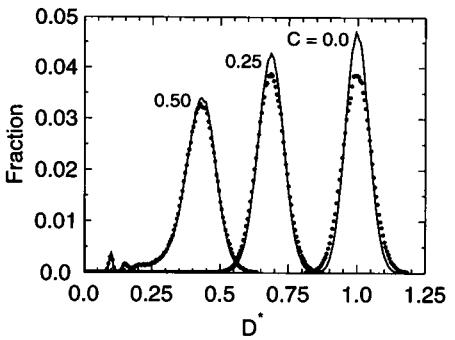

FIGURE A6 Distributions of the short-range diffusion coefficient $D^*(0{:}4)$ calculated by unweighted least-squares fits for averages over all pairs (*lines*) and all independent pairs (*points*).

where $u = z\,N_I/4Dt$, and Γ is the gamma function. The variance is

$$\mathrm{Var}\,\langle r^2\rangle_I = (4Dt)^2/N_I. \tag{A6}$$

For an average over all segments (Qian et al., 1991),

$$\mathrm{Var}\,\langle r^2\rangle_A = (4Dt)^2F, \tag{A7}$$

where for $N_A \geq n$,

$$F = (n^2N_A + 2N_A + n - n^3)/(6nN_A^2) \tag{A8}$$

and for $N_A \leq n$,

$$F = 1 + (N_A^3 - 4nN_A^2 + 4n - N_A)/(6n^2N_A). \tag{A9}$$

Fig. A2 shows the standard deviations σ_I and σ_A normalized by the SD for the unaveraged case, for a 256-step random walk. The standard deviations for the two averages are similar. The jumps in σ_I are a result of the greatest integer function in Eq. A1, and the values of σ_I at the jumps are large, because the last segment of the trajectory is too short to contribute to the average, and those points are discarded.

Fig. A3 shows the standard deviations σ_A for the average over all pairs as $\langle r^2(t)\rangle \pm \sigma_A$ and $\langle r^2(t)\rangle \pm 2\sigma_A$. Such a figure has been shown several times before (Qian et al., 1991; Fein et al., 1993; Hicks and Angelides, 1995), but it is repeated here to emphasize the magnitude of the SD for times of half the trajectory length or more. As Fig. A2 indicates, the corresponding plot for averages over independent pairs would be very similar.

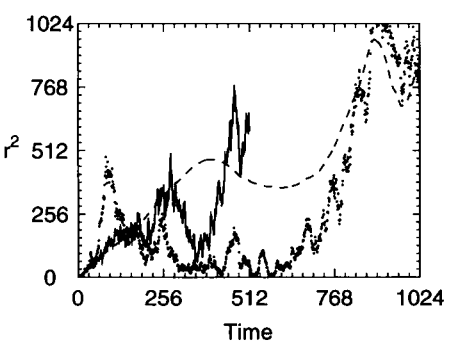

FIGURE A5 Averaging of a single trajectory. Dots indicate the square displacement $r^2(t)$ for one trajectory, an unobstructed random walk of 1024 time steps on a triangular lattice. The solid line indicates the MSD $\langle r^2(t)\rangle_I$ averaged over independent pairs. The dashed line indicates $\langle r^2(t)\rangle_A$ averaged over all pairs.

In calculating the diffusion coefficient by a least-squares fit to the MSD versus t curve, the weight of the ith point is $1/\mathrm{Var}_i$, where Var_i is the variance of the ith point. Weights for a trajectory of 1024 time steps are shown in Fig. A4. The weights fall off very rapidly with the lag time, and the difference between the two averages is small.

Fig. A5 shows $r^2(t)$, $\langle r^2(t)\rangle_A$, and $\langle r^2(t)\rangle_I$ for a single trajectory. At short time lags, the averages agree well. At large time lags, the averages over all pairs are smoother than the averages over independent pairs, but low-frequency fluctuations are still present, corresponding to the large standard deviations of Fig. A3. The two averages may disagree at large time lags, but one should not use either average at large time lags.

Finally, Fig. A6 compares the distributions of the short-range diffusion coefficient for the two averages. The distribution for the average over all pairs is slightly narrower, but the difference is insignificant in SPT experiments. Similar histograms for the binding models of Fig. 7 show little difference in D^* for the two averages. If weighted averages are used, the distributions are even closer, and for intermediate-range diffusion coefficients (128 time points) the distributions are indistinguishable. Examination of the ratio D_A/D_I for an unobstructed continuum random walk of 1024 time steps showed that the short-range diffusion coefficients for individual trajectories agreed well.

In summary, we recommend averaging over all pairs, because this average uses all the data, and it weights the data points nearly equally. (We cannot exclude the possibility that other anomalous diffusion models exist for which the average over all pairs is inappropriate.) The difference in the two averages is small for small time lags, and at large time lags neither average is able to tame the fluctuations in a random walk. One should cut off the average at a maximum lag time of, say, one-quarter of the total number of time steps.

I thank Hong Qian and Watt W. Webb for helpful discussions.

This work was supported by National Institutes of Health grant GM38133.

REFERENCES

Almeida, P. F. F., and W. L. C. Vaz. 1995. Lateral diffusion in membranes. *In* Structure and Dynamics of Membranes, Vol. 1. R. Lipowsky and E. Sackmann, editors. Elsevier Science, Amsterdam. 305–357.

Bergelson L. D., K. Gawrisch, J. A. Ferretti, and R. Blumenthal. 1995. Domain organization in biological membranes. *Mol. Membr. Biol.* 12: 1–162.

Bevington, P. R., and D. K. Robinson, 1992. Data Reduction and Error Analysis for the Physical Sciences, 2nd ed. McGraw-Hill, New York. 101–104.

Bouchaud, J.-P., and A. Georges. 1988. The physical mechanisms of anomalous diffusion. *In* Disorder and Mixing. E. Guyon, J.-P. Nadal, and Y. Pomeau, editors. Kluwer Academic Publishers, Dordrecht. 19–29.

Bouchaud, J.-P., and A. Georges. 1990. Anomalous diffusion in disordered media: statistical mechanisms, models and physical applications. *Phys. Rep.* 195:127–293.

Braun, M., and K. W. Kehr. 1990. Diffusivity and mobility of lattice gases in lattices with randomly blocked sites. *Phil. Mag. A* 61:855–871.

Bunde, A. 1988. Anomalous transport in disordered media. *Solid State Ionics, Diffusion & Reactions* 28-30:34–40.

Carslaw, H. S., and J. C. Jaeger. 1959. Conduction of Heat in Solids, 2nd ed. Clarendon Press, Oxford. 258.

Edidin, M. 1992. Translational diffusion of membrane proteins. *In* The Structure of Biological Membranes. P. Yeagle, editor. CRC Press, Boca Raton. 539–571.

Edidin, M. 1993. Patches and fences: probing for plasma membrane domains. *J. Cell Sci. Suppl.* 17:165–169.

Edidin, M. 1994. Fluorescence photobleaching and recovery, FPR, in the analysis of membrane structure and dynamics, *In* Mobility and Proximity in Biological Membranes. S. Damjanovich, J. Szöllősi, L. Trón, M. Edidin, editors. CRC Press, Boca Raton, 109–135.

Feder, T. J., I. Brust-Mascher, J. P. Slattery, B. Baird, and W. W. Webb. 1996. Constrained diffusion or immobile fraction on cell surfaces: a new interpretation. *Biophys. J.* 70:2767–2773.

Fein, M., J. Unkeless, F. Y. S. Chuang, M. Sassaroli, R. da Costa, H. Väänänen, and J. Eisinger. 1993. Lateral mobility of lipid analogues and GPI-anchored proteins in supported bilayers determined by fluorescent bead tracking. *J. Membr. Biol.* 135:83–92.

Ghosh, R. N. 1991. Mobility and clustering of individual low-density lipoprotein receptor molecules on the surface of human skin fibroblasts. Ph.D. thesis. Cornell University, Ithaca. 260 pp.

Ghosh, R. N., and W. W. Webb. 1994. Automated detection and tracking of individual and clustered cell surface low density lipoprotein receptor molecules. *Biophys. J.* 66:1301–1318.

Gnedenko, B. V. 1968. The Theory of Probability. 4th ed. Chelsea Publishing Co., New York. 183–185.

Gordon, G. W., B. Chazotte, X. F. Wang, and B. Herman. 1995. Analysis of simulated and experimental fluorescence recovery after photobleaching. Data for two diffusing components. *Biophys. J.* 68:766–778.

Haus, J. W., and K. W. Kehr. 1987. Diffusion in regular and disordered lattices. *Phys. Rep.* 150:263–406.

Havlin, S., and D. Ben-Avraham. 1987. Diffusion in disordered media. *Adv. Phys.* 36:695–798.

Hicks, B. W., and K. J. Angelides. 1995. Tracking movements of lipids and Thy1 molecules in the plasmalemma of living fibroblasts by fluorescence video microscopy with nanometer scale precision. *J. Membr. Biol.* 144:231–244.

Jacobson, K., D. O'Dell, and J. T. August. 1984. Lateral diffusion of an 80,000-dalton glycoprotein in the plasma membrane of murine fibroblasts: relationships to cell structure and function. *J. Cell Biol.* 99:1624–1633.

Jacobson, K., and Vaz, W. L. C., editors. 1992. Domains in biological membranes. *Comments Mol. Cell. Biophys.* 8:1–114.

Kusumi, A., and Y. Sako. 1996. Cell surface organization by the membrane skeleton. *Curr. Opin. Cell Biol.* 8:566–574.

Kusumi, A., Y. Sako, and M. Yamamoto. 1993. Confined lateral diffusion of membrane receptors as studied by single particle tracking (nanovid microscopy). Effects of calcium-induced differentiation in cultured epithelial cells. *Biophys. J.* 65:2021–2040.

Lee, G. M., A. Ishihara, and K. A. Jacobson. 1991. Direct observation of Brownian motion of lipids in a membrane. *Proc. Natl. Acad. Sci. USA.* 88:6274–6278.

Lee, G. M., F. Zhang, A. Ishihara, C. L. McNeil, and K. A. Jacobson. 1993. Unconfined lateral diffusion and an estimate of pericellular matrix viscosity revealed by measuring the mobility of gold-tagged lipids. *J. Cell Biol.* 120:25–35.

Munnelly, H. M., W. F. Wade, D. A. Roess, and B. G. Barisas. 1996. Interferometric fringe pattern photobleaching recovery measurements interrogate entire cells. *Biophys. J.* 70:447*a* (Abstr.).

Nagle, J. F. 1992. Long tail kinetics in biophysics? *Biophys. J.* 63: 366–370.

Petersen, N. O., S. Felder, and E. L. Elson. 1986. Measurement of lateral diffusion by fluorescence photobleaching recovery. *In* Handbook of Experimental Immunology: Vol. 1. Immunochemistry, D. M. Weir, editor. Blackwell Scientific Publications, Oxford. 24.1–24.23

Press, W. H., S. A. Teukolsky, W. T. Vetterling, and B. P. Flannery. 1992. Numerical Recipes in Fortran: The Art of Scientific Computing, 2nd ed. Cambridge University Press, Cambridge. 277–279.

Qian, H., M. P. Sheetz, and E. L. Elson. 1991. Single particle tracking. Analysis of diffusion and flow in two-dimensional systems. *Biophys. J.* 60:910–921.

Sako, Y., and A. Kusumi. 1994. Compartmentalized structure of the plasma membrane for receptor movements as revealed by a nanometer-level motion analysis. *J. Cell Biol.* 125:1251–1264.

Saxton, M. J. 1995. Single-particle tracking: effects of corrals. *Biophys. J.* 69:389–398.

Saxton, M. J. 1996. Anomalous diffusion due to binding: a Monte Carlo study. *Biophys. J.* 70:1250–1262.

Saxton, M. J., and K. Jacobson. 1997. Single-particle tracking: applications to membrane dynamics. *Annu. Rev. Biophys. Biomol. Struct.* In press.

Scalettar, B. A., and J. R. Abney. 1991. Molecular crowding and protein diffusion in biological membranes. *Comments Mol. Cell. Biophys.* 7:79–107.

Scher, H., M. F. Shlesinger, and J. T. Bendler. 1991. Time-scale invariance in transport and relaxation. *Phys. Today* 44(1):126–34.

Schram, V., H.-N. Lin, and T. E. Thompson. 1996. Topology of gel-phase domains and lipid mixing properties in phase-separated two-component phosphatidylcholine bilayers. *Biophys. J.* 71:1811–1822.

Schram, V., J. F. Tocanne, and A. Lopez. 1994. Influence of obstacles on lipid lateral diffusion: computer simulation of FRAP experiments and application to proteoliposomes and biomembranes. *Eur. Biophys. J.* 23:337–348.

Slattery, J. P. 1995. Lateral mobility of FcεRI on rat basophilic leukemia cells as measured by single particle tracking using a novel bright fluorescent probe. Ph. D. thesis. Cornell University, Ithaca. 153 pp.

Thomas, J., and W. W. Webb. 1990. Fluorescence photobleaching recovery: a probe of membrane dynamics. *In* Noninvasive Techniques in Cell Biology. J. K. Foskett and S. Grinstein, editors. Wiley-Liss, New York. 129–152.

Tocanne, J. F., L. Cézanne, A. Lopez, B. Piknova, V. Schram, J. F. Tournier, and M. Welby. 1994a. Lipid domains and lipid/protein interactions in biological membranes. *Chem. Phys. Lipids* 73:139–158.

Tocanne, J. F., L. Dupou-Cézanne, and A. Lopez. 1994b. Lateral diffusion of lipids in model and natural membranes. *Prog. Lipid Res.* 33:203–237.

Wade, W. F., J. H. Freed, M. Edidin. 1989. Translational diffusion of class II major histocompatibility complex molecules is constrained by their cytoplasmic domains. *J. Cell Biol.* 109:3325–3331.

Welti, R, and M. Glaser. 1994. Lipid domains in model and biological membranes. *Chem. Phys. Lipids* 73:121–137.

Zhang, F., G. M. Lee, and K. Jacobson. 1993. Protein lateral mobility as a reflection of membrane microstructure. *Bioessays.* 15:579–588.